Role of density fluctuations in the relaxation of random dislocation systems

Ferenc F
 Csikor $^{1,2},$ Michael Zaiser 2, Péter Dus
án Ispánovity 1 and István Groma 1

- Department of Materials Physics, Eötvös Loránd University, Pázmány Péter sétány 1/a, H-1117 Budapest, Hungary
- 2 Centre for Materials Science and Engineering, The University of Edinburgh, The King's Buildings, Edinburgh EH9 3JL, United Kingdom

E-mail: csikor@metal.elte.hu, M.Zaiser@ed.ac.uk, ispanovity@metal.elte.hu, groma@metal.elte.hu

Abstract. We study the relaxation dynamics of systems of straight, parallel crystal dislocations, starting from initially random and uncorrelated positions of the individual dislocations. A scaling model of the relaxation process is constructed by considering the gradual extinction of the initial density fluctuations present in the system. The model is validated by ensemble simulations of the discrete dynamics of dislocations. Convincing agreement is found for systems of edge dislocations in single slip irrespective of the net Burgers vector of the dislocation system. It is also demonstrated that the model does not work in multiple slip geometries.

PACS numbers: 61.72.Lk, 05.40.-a, 45.50.Jf, 62.20.fq

Keywords: defects (theory), fluctuations (theory), plasticity (theory)

1. Introduction

The creation and motion of large numbers of crystal lattice dislocations is the most fundamental feature of crystal plasticity. During the last half century, the physical properties of individual dislocations and their interactions with localised obstacles have been studied extensively. On the other hand, the complex collective dynamics of strongly interacting many-dislocation systems is still far from being understood. Fortunately, everyday plastic deformation processes very often proceed orders of magnitude slower than the typical relaxation times of the underlying dislocation system. These conditions often permit to study the problem in a quasistatic approximation [1, 2]. Beyond the quasistatic limit, however, much less work has been devoted to studying the dynamics of collective dislocation motions which lead to the formation of metastable configurations, and to transitions between such configurations in driven dislocation systems. However, such collective motions are crucial for understanding rapid dislocation processes which not only occur in shock loading but, in the form of dislocation avalanches, are a generic feature of the dynamics of driven dislocation systems [3].

The first studies of dynamic relaxation processes in dislocation systems were performed by Miguel et al. with the protocol of applying a constant external shear stress to well relaxed dislocation configurations [4, 5, 6]. The ensuing creep relaxation was numerically shown to follow Andrade's law stemming from the underlying intermittent and correlated motion of dislocation structures. The connection between the mesoscopic and macroscopic features of the process was, however, not analysed in detail.

Another direction was taken by the present authors who conducted systematic studies of the relaxation dynamics of initially random configurations of straight dislocations. This is an important issue since the elastic energy density \mathcal{E} of a random dislocation system of density ρ is known to diverge with the logarithm of system size L, $\mathcal{E} \propto \rho \ln(L/b)$ [7] where b is the modulus of the dislocation Burgers vector. In a well-relaxed dislocation arrangement, on the other hand, the same quantity scales like $\mathcal{E} \propto \rho \ln(1/(b\sqrt{\rho}))$, i.e., the screening length corresponds to the mean dislocation spacing [8, 9, 10]. As the mean square stress is proportional to the elastic energy density, this screening also removes a logarithmic divergence of the width of the internal stress probability distribution [11], and of the X-ray line width [10, 11, 12]. Numerical experience showed that, at least in single slip geometries, the relaxation processes that lead to screened dislocation arrangements exhibit slow, power law characteristics for quantities such as the elastic energy or the average dislocation velocity [13]. A model was proposed which relates the power-law relaxation dynamics to the gradual extinction of initial dislocation density fluctuations [14]. The present paper presents a comprehensive numerical investigation which allows to check in detail the model predictions and complements the earlier work by extending the investigation to multiple slip geometries and to dislocation systems of non-zero net Burgers vector, and by studying the influence of an external driving stress on the relaxation process.

The paper is organised as follows. In section 2 the problem is defined and technical

details of the simulations are presented. Section 3 unfolds a scaling model of the relaxation process from a chemical analogy and uses this model to predict the evolution of simulation measurables. Section 4 then gives a detailed comparison between model predictions and numerical results. The results are discussed and conclusions are drawn in section 5. An auxiliary calculation of the elastic energy of a random dislocation wall is presented in the Appendix.

2. Problem definition and simulations

2.1. Equations of motion

Consider a system of N straight edge dislocations running parallel to the z axis of a Cartesian coordinate system. Let all dislocations have a common Burgers vector pointing along the x axis (a so-called single slip geometry), $\mathbf{b}_i = s_i b \mathbf{e}_x$, where $s_i = \pm 1$ is the sign of the ith dislocation. Assuming overdamped glide motion with a dislocation velocity v that is proportional to the local resolved shear stress, and zero dislocation mobility in the climb direction, the equation of motion of dislocation i piercing the xy plane at $\mathbf{r}_i = (x_i, y_i)$ can be written as

$$\dot{x}_i = \chi b s_i \left[\sum_{j \neq i} s_j \tau_{\text{ind}}(\boldsymbol{r}_i - \boldsymbol{r}_j) + \tau_{\text{ext}} \right], \qquad \tau_{\text{ind}}(\boldsymbol{r}) = G b \frac{x(x^2 - y^2)}{(x^2 + y^2)^2}, \qquad (1)$$

where χ denotes the dislocation glide mobility, $G = \mu/[2\pi(1-\nu)]$ where μ is the shear modulus and ν is Poisson's ratio of the embedding isotropic crystal, $\tau_{\rm ind}(\mathbf{r})$ denotes the resolved shear stress field induced by a positive dislocation located at the origin [15], and $\tau_{\rm ext}$ is a constant externally applied resolved shear stress.

It is useful to introduce natural coordinates at this point which will be denoted by an apostrophe (') in the following. Measuring length in units of the average dislocation—dislocation distance $\rho^{-1/2}$ (where ρ denotes the total dislocation density of dislocations including both signs and, in multiple slip geometries, including all slip systems), stress τ in units of $Gb\sqrt{\rho}$, and plastic strain γ in units of $b\sqrt{\rho}$ leads to the relations

$$x' = x\sqrt{\rho}, \qquad t' = t\rho\chi Gb^2, \qquad \tau' = \tau/(Gb\sqrt{\rho}),$$

$$v' = v/(\sqrt{\rho}\chi Gb^2), \qquad \gamma' = \gamma/(b\sqrt{\rho}), \qquad \Delta E' = \Delta E/(Gb^2),$$
 (2)

where ΔE is the elastic energy difference between two states of the system (energy per unit dislocation length). In natural coordinates (1) takes the form

$$\dot{x}'_{i} = s_{i} \left[\sum_{j \neq i} s_{j} \tau'_{\text{ind}} (\boldsymbol{r}'_{i} - \boldsymbol{r}'_{j}) + \tau'_{\text{ext}} \right],$$

$$\tau'_{\text{ind}} (\boldsymbol{r}') = \frac{x'(x'^{2} - y'^{2})}{(x'^{2} + y'^{2})^{2}} = \frac{\cos(\varphi)\cos(2\varphi)}{r'},$$
(3)

where φ denotes the angle between the x axis and r'.

2.2. Simulation details

To study dislocation relaxation, a large number of discrete dislocation dynamics simulations have been performed. Equations of motion (3) were solved with the 4.5th order Runge–Kutta–Fehlberg method. Periodic boundary conditions were applied to a square simulation area with edges parallel to the slip planes, following the method used in [16].

To avoid overly small timesteps during the final stages of approach of narrow dipoles (pairs of dislocations of opposite signs), a small number of extremely narrow dipoles were excluded from the solution of (3) and forced to move as if they were isolated from the rest of the system. This is justified as the far-field stresses of the dislocations in a narrow dipole cancel, while their pair interaction diverges when the dislocation-dislocation distance approaches zero. As a consequence, the dynamics of narrow dipoles is effectively uncoupled from the rest of the dislocation system. We do not allow for annihilation of narrow dipoles, which is a process that is governed by the atomistics of the dislocation cores. This implies that we consider dislocation spacings to be large in comparison with the dipole annihilation distance, which is believed to be of the order of one nanometer. As typical dislocation densities in highly dislocated crystals are of the order of 10^{14} m⁻², i.e. the average dislocation spacings are of the order of a hundred nanometers, this is not a severe restriction.

A first set of simulations was started from random configurations of equal numbers of positive and negative dislocations. The number of simulated dislocations N (which defines the system size $L_{\rm s}'$ since $N=L_{\rm s}'^2$) varied between 16 and 128. It is well known that the flow stress of single-glide dislocation systems is around 0.1 in natural units [4]. To allow the dislocation systems to reach mechanical equilibrium at the end of the relaxation, we restricted the applied external stresses to levels below the flow stress, using stresses between 0 and 0.088 natural units.

As seen in figure 1, individual simulations showed strong avalanche-like activity during relaxation, as previously observed in [5]. To reveal scaling properties of the relaxation process, the evolution of global parameters such as stored energy, mean absolute dislocation velocity, mean square velocity, and mean strain rate was averaged over 3600 to 10⁵ simulations starting from different random initial configurations. This ensemble averaging resulted in smooth ensemble averaged graphs as seen in figure 1.

In addition to the relaxation of 'neutral' arrangements of dislocations moving on a single slip system aligned parallel to the edge of a square simulation area, we considered two variants of this basic setting (these simulations were only performed at zero external stress): i) To elucidate the influence of different implementations of the boundary conditions, we performed single slip simulations with the simulation box oriented at an angle φ to the slip planes. This does not affect the short-range dislocation—dislocation interactions but modifies the stress field created by the periodic images. ii) To study the influence of a net Burgers vector on the relaxation process, we investigated the limiting case of fully polarised dislocation systems (dislocations of one sign only) of

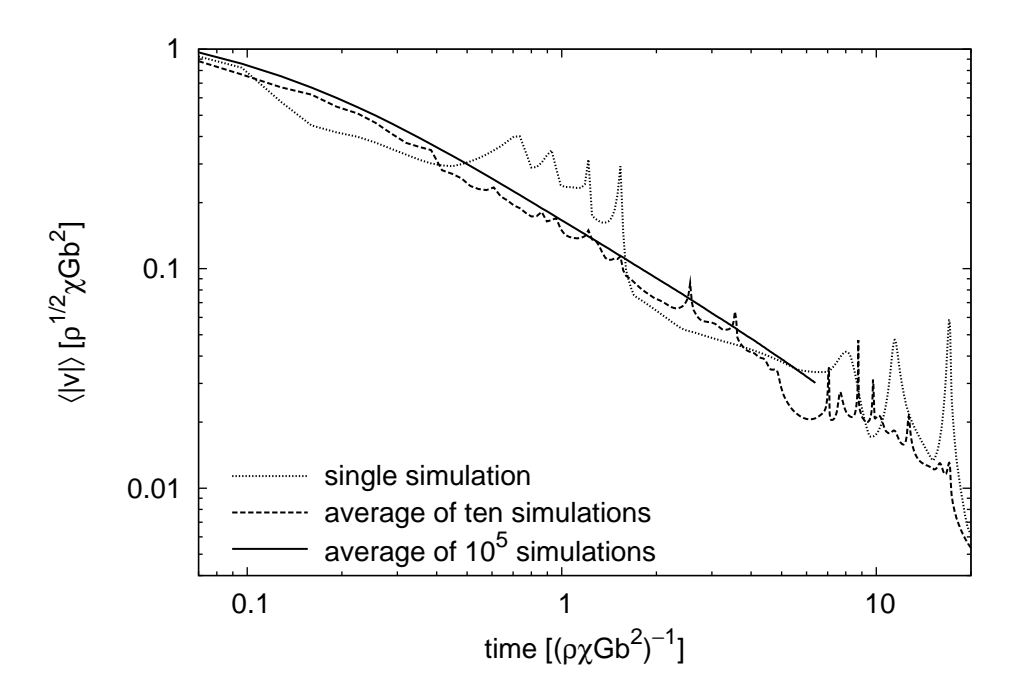


Figure 1. Evolution of the average dislocation velocity for different ensemble sizes.

sizes 16 < N < 128.

To investigate the differences between single and multiple slip geometries, we also performed simulations in which dislocations of multiple slip systems were present. In these simulations we considered sets of equally populated slip systems, each containing edge dislocations with a zero net Burgers vector that were initially distributed at random. The methodology of the multiple slip simulations was identical to the single slip simulations described above, with the following differences: i) For each dislocation in the system, the complete elastic stress tensor was computed, again assuming periodic boundary conditions in a square simulation area and using the method of [16]. The forces acting on the dislocations were calculated from the stress tensor components using the Peach-Koehler formula [15]. ii) In addition to narrow dipoles, which were treated in the same way as described above, pairs of attracting dislocations on intersecting slip planes needed to be treated separately. Such dislocation pairs react with each other and form a reaction product ('dislocation lock') with Burgers vector equal to the net Burgers vector of the constituent dislocations. In real crystals, both the mobility of dislocation locks and the stress required for separating them into the constituent dislocations depend on their atomic core structure. For simplicity, we assumed all dislocation locks to be immobile and to possess infinite separation stress. New dislocations joining an existing lock were assumed to annihilate with the constituent dislocation of the opposite Burgers vector if such a dislocation was present. If a dislocation lock converted to an ordinary dislocation through such an annihilation event, it was assumed to become mobile again. To avoid overly small timesteps during the final stages of dislocation lock formation or reaction with a new dislocation (again due to diverging elastic interactions between the constituent dislocations) the moving constituent dislocations were pinned when their relative distance decreased below a small predefined reaction radius which mimics the core extension of the dislocation lock. For simplicity, the stress field of a lock was calculated as the superposition of the stress fields of the pinned constituent dislocations. Although the positions of the constituent dislocations are scattered over a small region of the size of the reaction radius, their net stress field is a good approximation of the stress field of the lock at larger distances. Finally, we note that this stress field is of long range character since the net Burgers vector of a dislocation lock is not zero.

3. Theory

In this section a simple scaling argument is used to establish the asymptotic kinetics of a bimolecular combination reaction. We then adapt the fundamental ideas behind this argument to the relaxation of dislocation systems as described in the previous section. Based on the adapted model, predictions are made for the evolution of several physical quantities which can be directly obtained from the simulations described in section 2. These predictions are compared in detail to the numerical results in section 4.

3.1. Role of density fluctuations in bimolecular reaction kinetics

Consider the direct combination reaction

$$A + B \rightarrow C$$
 (4)

starting from a random, balanced configuration of the two reactants

$$\bar{c}_{\mathrm{A}}^{0} = \bar{c}_{\mathrm{B}}^{0},\tag{5}$$

where \bar{c} denotes the spatial average of the concentration field c(r). Note that the initial concentrations of molecules A and B are equal only in an average sense because of the thermally induced random positions of the individual molecules. These concentration fluctuations need to be taken into account when modelling the reaction kinetics. For situations where long-distance transport of particles occurs by free Brownian motion, a simple scaling argument which captures the essential physics was given by Ovchinnikov [17] (which the reader is advised to consult for further details). Broadly speaking, this involves the subsequent dominance of two consecutive mechanisms directly corresponding to the different length scales inherent in the system: i) the reaction of those molecules that do not need long distance motion to find a reaction partner, followed by ii) the long range Brownian motion and subsequent reaction of excess reactants remaining as a result of initial concentration fluctuations.

3.1.1. Stage 1: Reaction controlled kinetics. As discussed in [17], the first stage of reaction (4) is controlled by a bimolecular reaction rate k which depends on the short-range interactions between the reaction partners. This stage can be discussed in the classical approximation

$$\dot{\bar{c}}_{A} = \dot{\bar{c}}_{B} = -k\bar{c}_{A}\bar{c}_{B}.\tag{6}$$

Solving (6) for initial conditions (5) yields

$$\bar{c}_{A} = \bar{c}_{B} = \frac{\bar{c}_{A}^{0}}{1 + k\bar{c}_{A}^{0}t}, \qquad t \ge 0,
\bar{c}_{A} = \bar{c}_{B} = (kt)^{-1}, \qquad t \gg (k\bar{c}_{A}^{0})^{-1}.$$
(7)

3.1.2. Stage 2: Diffusion controlled kinetics. Because of thermal concentration fluctuations, not all of the molecules A and B can be consumed during stage 1. Spatial fluctuations of the reactant concentrations lead to local excess of molecules of one type. As these excess molecules cannot find a local partner, they need to migrate via long range Brownian motion, leading to a second kinetic stage controlled by long-range diffusion.

To characterise the concentration fluctuations in question we observe that, on scales larger than the range of the 'contact interactions' which govern the first stage of the reaction kinetics, the positions of molecules are statistically independent. As a consequence, the initial numbers of molecules A or B in a sufficiently large volume V are Poisson distributed. This implies that the mean numbers of excess molecules fulfil the relations [17]

$$\left(\bar{N}_{A,\text{excess}}^{0,V}\right)^{2} = V^{2} \langle (c_{A}(\boldsymbol{r}) - \bar{c}_{A}^{0})^{2} \rangle = V \bar{c}_{A}^{0},
\left(\bar{N}_{B,\text{excess}}^{0,V}\right)^{2} = V^{2} \langle (c_{B}(\boldsymbol{r}) - \bar{c}_{B}^{0})^{2} \rangle = V \bar{c}_{B}^{0},$$
(8)

where $\langle \rangle$ denotes spatial averaging over a large statistically homogeneous system or, equivalently, ensemble averaging over a large number of statistically independent and equivalent realizations.

To further discuss the reaction kinetics during stage 2, we confine ourselves to the limiting case of an infinite bimolecular reaction rate $k \to \infty$. This choice does not affect the generality of the discussion, it only affects the moment of the crossover between stage 1 and stage 2 kinetics. We introduce the concentration difference $z(\mathbf{r})$ as

$$z(\mathbf{r}) = c_{\mathbf{A}}(\mathbf{r}) - c_{\mathbf{B}}(\mathbf{r}). \tag{9}$$

In a hypothetical initial state before the reaction has been 'switched on' at t = 0, $c_{\rm A}(\mathbf{r})$ and $c_{\rm B}(\mathbf{r})$ are statistically independent and $z(\mathbf{r})$ has the initial statistical properties [17]

$$\langle z(\mathbf{r}) \rangle = \langle c_{\mathbf{A}}(\mathbf{r}) - c_{\mathbf{B}}(\mathbf{r}) \rangle = 0,$$

$$\langle z(\mathbf{r})^{2} \rangle = \langle (c_{\mathbf{A}}(\mathbf{r}) - c_{\mathbf{B}}(\mathbf{r}))^{2} \rangle = 2\bar{c}_{\mathbf{A}}^{0}/V = 2\bar{c}_{\mathbf{B}}^{0}/V.$$
(10)

To proceed, we note that for $k \to \infty$ molecules A and B cannot coexist for t > 0. Therefore, $z(\mathbf{r})$ gives a complete characterisation of the concentration map for t > 0: for $z(\mathbf{r}) > 0$, $c_{\rm A}(\mathbf{r}) = z(\mathbf{r})$ and $c_{\rm B}(\mathbf{r}) = 0$ and for $z(\mathbf{r}) < 0$, $c_{\rm A}(\mathbf{r}) = 0$ and $c_{\rm B}(\mathbf{r}) = -z(\mathbf{r})$. Because there exists no other physical length scale in the system, the size of the regions characterised by z > 0 and z < 0 is determined by the diffusion length $L(t) = \sqrt{Dt}$ (for simplicity, the same diffusion constant D is assumed for both kinds of reactants).

Consider now the volume referring to the diffusion length at time t, $V(t) = L(t)^3 = (Dt)^{3/2}$. One can suppose that for lengths larger than L(t) the fluctuations of $z(\mathbf{r})$ are still not affected by diffusion; therefore, one can write that

$$\langle |z(\mathbf{r})| \rangle \approx (\bar{c}_{A}^{0}/V(t))^{1/2} = (\bar{c}_{A}^{0})^{1/2} D^{-3/4} t^{-3/4}.$$
 (11)

In some regions, $c_{\rm A}(\mathbf{r}) = |z(\mathbf{r})|$ and in others, $c_{\rm B}(\mathbf{r}) = |z(\mathbf{r})|$; hence, on average

$$\bar{c}_{A}(t) = \bar{c}_{B}(t) = \frac{1}{2} \langle |z| \rangle \approx (\bar{c}_{A}^{0})^{1/2} D^{-3/4} t^{-3/4},$$
 (12)

meaning a slower kinetics than in stage 1 (7). (For a more detailed derivation see [17]).

Note that (12) is only applicable within certain time limits $[t_1, t_2]$. For instance, for $k \to \infty$, t_1 is equal to the time the diffusion length L(t) needs to exceed the average intermolecular distance. t_2 is determined by the time needed by L(t) to reach the system size L_s , independent of the value of k.

3.2. Role of density fluctuations in the relaxation of random dislocation configurations

3.2.1. Analogy between chemical and dislocation systems. Now we consider the relaxation of initially random dislocation configurations with the same number of positive and negative dislocations ($\sum_i s_i = 0$) following the equations of motion (3). Although not immediately evident, this relaxation process has strong phenomenological similarities to the kinetics of the chemical reaction described in section 3.1.

To elucidate the analogy, the relaxation process will be envisaged as a gradual screening of the long range elastic stress fields of individual dislocations through the formation of dislocation–dislocation correlations [9, 18]. We first envisage 'neutral' arrangements where dislocations of both signs are present in equal amounts. In a screened dislocation arrangement, the excess of one sign over the other has been eliminated on scales above a few dislocation spacings. Any dislocation arrangement where excess dislocations are completely eliminated can be envisaged as an assembly of dipoles where each dislocation has exactly one partner of opposite sign within a distance of the order of $\rho^{-1/2}$, and this picture will be used in the following argument. Hence, we envisage the relaxation process as the gradual formation of a large number of dislocation dipoles consisting of dislocations of opposite signs, i.e., as a bimolecular reaction process analogous to the chemical reaction (4).

The principal difference between the two processes lies in the dynamics of individual particles: for the dislocation system, dislocation glide motion is driven by dislocation—dislocation interactions which scale like 1/r, whereas in case of the chemical reaction we are dealing with diffusive Brownian motion of the reactants. Despite this difference, we may again construct a two-stage model for the dislocation relaxation process: i) in stage 1 adjacent opposite sign dislocations form dipoles; ii) in stage 2 initial fluctuations in the excess dislocation density gradually die out from shorter towards longer length scales as excess dislocations which did not find a dipole partner in stage 1 undergo long range glide motion. The process terminates once the length scale on which fluctuations have been eliminated reaches the system size.

3.2.2. Relaxation dynamics. To understand the time evolution of the system, we again consider the evolution of the typical length scale L(t) below which density fluctuations have already died out. To this end we consider that i) similar to the chemical case, areas

of size $L(t)^2$ typically contain mobile excess dislocations (which have still not 'reacted' into dipoles) with only one or the other sign and that ii) dislocation dipoles give rise only to short range stress fields with a $1/r^2$ decay. As the typical distance between opposite sign dislocations which try to find each other is proportional to L'(t'), the typical driving stress towards dipole formation scales as $\tau' \sim 1/L'(t')$. (Recall that variables with an apostrophe (') are measured in natural units.) The dislocation velocity is proportional to τ' , and therefore the characteristic time for eliminating excess dislocations on scale L' scales as $L'/\tau' \propto (L')^2$. Hence we find that

$$\frac{\mathrm{d}L'}{\mathrm{d}t'} \sim \frac{1}{L'}$$
 or, equivalently $L' \sim \sqrt{2t'}$. (13)

Incidentally, this result is very similar to the evolution law of L(t) for Brownian motion, $L = \sqrt{Dt}$. By supposing that the mobile dislocations inherit the initial concentration fluctuations we find that at time t', regions of size $L'(t')^2 \sim 2t'$ contain about L' excess dislocations of one or the other sign, and L'^2 dislocations in total (see the chemical model in section 3.1.2). Thus, the fraction of non-paired dislocations is estimated to decrease in time as

$$\frac{N_{\text{excess}}}{N} \sim \frac{L'}{L'^2} \sim \frac{1}{\sqrt{2t'}}.$$
 (14)

Following the chemical model in section 3.1.2, it is straightforward to predict the time interval $[t'_1, t'_2]$ during which the above argument is expected to hold. The start time t'_1 is characterised by L reaching the dislocation–dislocation distance $\rho^{-1/2}$ (1 in natural units) and the process is finished when L reaches the system size L_s . With (13) this leads to

$$t_1' \sim \frac{1}{2} \qquad t_2' \sim \frac{L_s'^2}{2} = \frac{\rho L_s^2}{2} = \frac{N}{2} \qquad \frac{t_2'}{t_1'} = \frac{t_2}{t_1} \sim N$$
 (15)

in natural coordinates where N denotes the total number of dislocations in the system.

3.2.3. Scaling relations for energy and velocity. The fraction of 'non-paired' dislocations is not a convenient quantity for comparing the scaling model with dislocation dynamics simulations, as the definition of 'dislocation pairs' in a multipolar dislocation arrangement may be ambiguous. Instead, we consider the evolution of the nth moment $\langle |v|^n \rangle$ of the dislocation velocity and of the excess elastic energy, both of which can be determined from the simulations in a straightforward manner. To obtain scaling estimates for the relaxation of these quantities, we assume that all dislocation dipoles are at rest and only the excess dislocations move. Furthermore, we assume that the motion of excess dislocations is not hindered by the dipoles already formed (this can be rationalised with the short range of the dipole stress field). The velocity of excess dislocations scales as $|v'| \sim 1/L'$, leading to

$$\langle |v'|^n \rangle \sim \frac{N_{\text{excess}}}{N} \times |v'|^n \sim \frac{1}{L'} \times \frac{1}{(L')^n} = (L')^{-(n+1)} \sim (2t')^{-(n+1)/2},$$
 (16)

where (13) and (14) have been used.

The dynamics of dislocations is assumed to be overdamped. Hence, the work that is done by the internal stresses in driving the system is completely dissipated: the amount of dissipated energy exactly matches the reduction in elastic energy. The energy dissipated per unit time by a moving dislocation i scales like $\tau_i v_i$ (the Peach–Koehler force acting on the dislocation is proportional to the stress), and consequently the time evolution of E can be expressed as

$$\Delta E'(t') = -\int_{t'}^{t'} \sum_{i=1}^{N} \tau_i'(t'') v_i'(t'') dt''.$$
(17)

Since the motion is overdamped, the dislocation velocity is proportional to the acting stress. In natural units and for $t' \in [t'_1, t'_2]$, the ensemble averaged elastic energy thus evolves like

$$\langle \Delta E' \rangle \propto -\int_{i=1}^{t'} \sum_{i=1}^{N} v_i'^2(t'') dt'' \approx -N \int_{i=1}^{t'} \langle v'^2 \rangle dt'' \approx -N \int_{i=1}^{t'} (2t'')^{-3/2} dt'' = N/\sqrt{2t'},$$
(18)

where (16) was used to estimate the time evolution of the second velocity moment.

Relaxation of arrangements of dislocations of the same sign. The scaling argument in the previous section is based on the formation of dipoles consisting of edge dislocations of opposite signs. At first glance, such an argument seems to be completely inapplicable to systems where only dislocations of the same sign are present. Dipole formation is clearly impossible in such systems. Instead, a most conspicuous feature in the relaxation of single-sign edge dislocation systems is the formation of walls containing many dislocations of the same sign that are aligned in the direction perpendicular to the slip plane [19]. Accordingly, theoretical arguments have focused on parameters characterising the 'condensation' of dislocations into walls [19]. However, even though dislocation wall formation is a most conspicuous feature, wall formation alone can not produce a screened dislocation arrangement. The authors of [19] evaluate the driving force for wall formation by assuming periodic spacing of dislocations along a wall and using classical results found e.g. in [15]. If we follow this line of reasoning and note that the energy of a dislocation in a wall decreases with decreasing dislocation spacing, the minimum-energy structure for the system at hand would be a single system-spanning wall. However, for an initially random dislocation system the y positions are independent random variables and it is not easy to see how a periodic arrangement could form in the absence of dislocation climb. We calculate the energy of a random wall in the Appendix and show that forming such a wall does not produce any energy reduction with respect to the initial random 2D arrangement.

How then can an arrangement of dislocations of the same sign be screened? The answer was provided by Wilkens [8] who demonstrated that a screened dislocation arrangement can be constructed by eliminating dislocation density fluctuations above a certain scale. To this end, he proposed a construction where the crystal cross section

is tiled into a grid of cells of size l, and the same number of dislocations is randomly distributed within each cell. This construction, which eliminates all density fluctuations on scales above the cell size, leads to an arrangement where the screening radius coincides with the cell size, $\mathcal{E} \propto \rho \ln(l/b)$.

Taking the Wilkens construction as a well-screened reference state offers a surprising outlook on the relaxation of initially random systems of same-sign dislocations. With respect to this reference state, the initial random arrangement contains density fluctuations on all scales which may be either positive ($\delta \rho = \rho(\mathbf{r}) - \langle \rho \rangle > 0$, positive excess) or negative ($\delta \rho < 0$, negative excess). To achieve screening, dislocations must migrate from regions of positive to regions of negative excess, and this process is governed by the long-range stress fields associated with the presence of (positive or negative) excess dislocations. In other words, the kinetics of the process follows from exactly the same scaling argument as used in the previous section: We are dealing with the stress-driven elimination of excess dislocation densities, with the only difference that the excess is now not of positive over negative dislocations, but of the local dislocation density over the average one.

If the above argument is correct, the relaxation kinetics of same-sign dislocation systems should be characterised by a slow power-law stage which has the same characteristics as the relaxation of neutral dislocation systems as discussed in the previous sections. We demonstrate in the next section that this is indeed the case.

4. Comparison with simulation results

4.1. Single slip relaxation of dislocation arrangements with zero net Burgers vector

4.1.1. Evolution of the elastic energy. The numerically determined evolution of the elastic energy is displayed in figure 2. The zero value of the energy was chosen to correspond to the final relaxed state of the system. As seen on the figure, the evolution of the elastic energy $\Delta E'/N$ per dislocation can be fitted satisfactorily with the prediction in (18), $\Delta E/N = A/\sqrt{2t'}$. Power-law relaxation occurs from times $t'_1 \approx 0.3$ onwards, in good agreement with the model prediction $t'_1 \sim 1/2$ in (15). The final equilibrium value of the elastic energy is not a priori known but was fitted to the data such as to achieve a maximum extension of the linear scaling regime. Unfortunately this precludes determination of the second critical time t'_2 from these results. The presence or absence of an external stress below the flow stress of the relaxed dislocation system seems to have negligible influence on the evolution of the elastic energy.

Note that it is possible to collapse the curves for different system sizes $L_{\rm s}'$ by normalising the graphs with $\ln(L_{\rm s}')$, as done in figure 2. This observation is consistent with the fact that the elastic energy of the initial random dislocation system is of the order of $E_0 \sim NGb^2 \ln(L_{\rm s}/b)$ while the energy of the final relaxed state is of the order of $E_{\infty} \sim NGb^2 \ln((\sqrt{\rho}b)^{-1})$ [7, 8]. For estimating the value of E_{∞} we used that the range of dislocation pair correlations in mechanical equilibrium is of the order of the mean

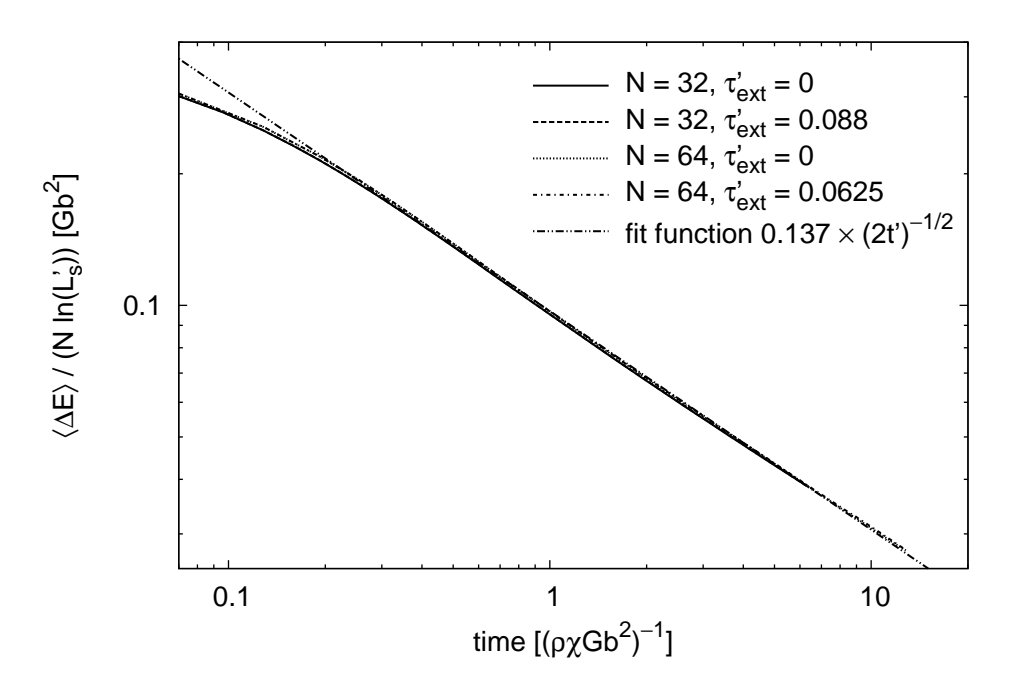


Figure 2. Evolution of the elastic energy per dislocation for different system sizes N and external stress values τ'_{ext} .

dislocation–dislocation distance $\rho^{-1/2}$ [9]. Therefore, the elastic energy difference per dislocation between the initial and final states is of the order of

$$\Delta E/N = (E_0 - E_{\infty})/N \sim Gb^2 \ln(L_s\sqrt{\rho}) = Gb^2 \ln(L_s').$$
 (19)

Despite this relation connecting the initial and final states of the system, the numerical finding that the $\Delta E(t)/N$ curves for different system sizes can be collapsed on their entire course by normalising them with $\ln(L'_{\rm s})$ is not trivial, as the agreement extends also to the relaxation kinetics and characteristic crossover time t'_1 .

4.1.2. Evolution of the mean square velocity. The numerically calculated evolution of the mean square velocity $\langle v'^2 \rangle$ is displayed in figure 3 for zero applied stress and different system sizes. Due to the connection (18) between the mean square velocity and the elastic energy of the system, it is not surprising that similar statements apply here as for the evolution of the elastic energy. As seen in the figure, the model prediction $\langle v'^2 \rangle \sim (2t')^{-3/2}$ in (16) fits the data well from $t'_1 \approx 0.3$. Due to the fact that $\langle v'^2 \rangle$ is proportional to the time derivative of the elastic energy, its graphs are much noisier than those obtained for the energy, preventing again the detection of the supposed upper critical time t'_2 . As for the energy, size effects can be scaled out with a normalisation factor $\ln(L'_{\rm s})^{-1}$ which is a direct consequence of (18) and (19). A final analogy to the evolution of the elastic energy is that external stresses have only negligible influence on the evolution of the mean square velocity. For this reason, simulations with non-zero external stresses were omitted from figure 3.

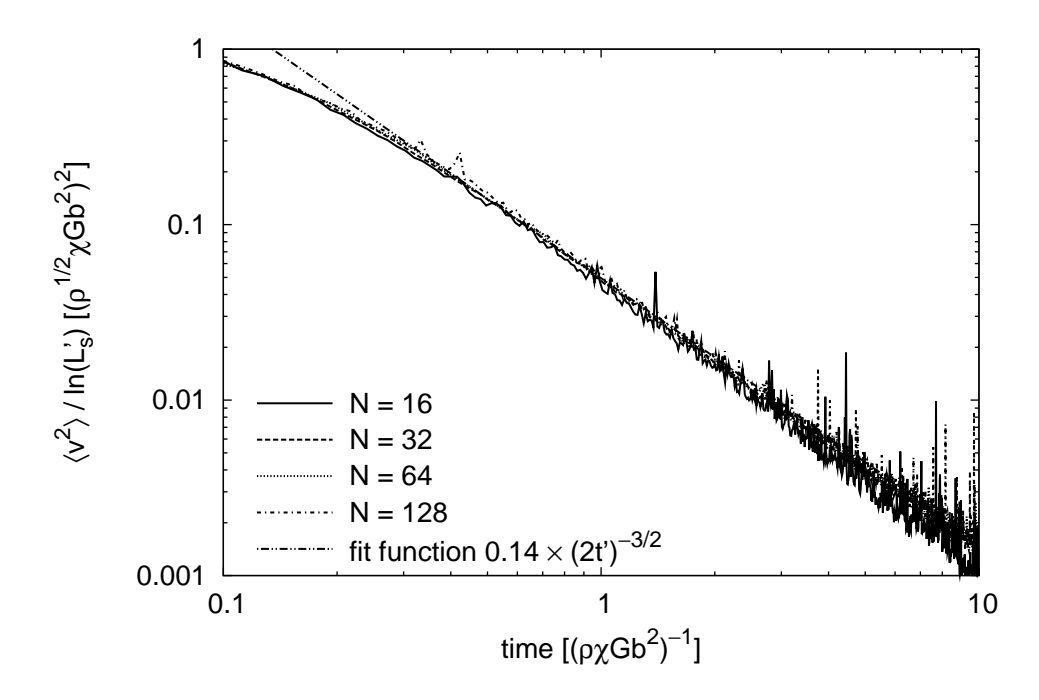


Figure 3. Evolution of the mean square velocity $\langle v'^2 \rangle$ for different system sizes N at zero external stress.

4.1.3. Evolution of the mean absolute velocity. In figure 4 the evolution of the mean absolute velocity $\langle |v'| \rangle$ can be seen for different system sizes. Again, a power law time dependence can be observed from $t'_1 \approx 0.3$ although an exponent -0.86 gives a better fit than the theoretically predicted -1 expected according to equation (16). One may argue that slowly moving dislocation dipoles play a bigger role in this case, as their small velocities contribute more strongly to $\langle |v'| \rangle$ than to $\langle v'^2 \rangle$. Therefore, the gradually increasing number of slowly moving dislocations might be responsible for the reduced relaxation exponent. What makes this figure very interesting is the possibility to estimate values of t'_2 . It was found that $t'_2 \approx 0.2N$ gives a good approximation, in line with the model prediction $t'_2 \sim N/2$ in (15). It was also observed that normalisation with $(\ln(L'_s))^{-1/2}$ collapses the graphs referring to different system sizes L'_s in the region of small $t' \ll t'_2$. This is consistent with the relations for the elastic energy and the mean square velocity. Finally, as in case of the energy and the mean square velocity, the evolution of the mean absolute velocity is not changed by the presence of external stresses below the macroscopic flow stress.

4.1.4. Evolution of the plastic strain rate. Another numerically measurable quantity is the plastic strain rate, defined as

$$\dot{\gamma} = \sum_{i} \frac{b_i \dot{x}_i}{L_s^2} = b L_s^{-2} \sum_{i} s_i \dot{x}_i \qquad \dot{\gamma}' = N^{-1} \sum_{i} s_i \dot{x}_i'. \tag{20}$$

In the following the evolution of $\dot{\gamma}'$ is studied for applied shear stresses $\tau'_{\rm ext}$ below the macroscopic flow stress for the present dislocation geometry. From the data of

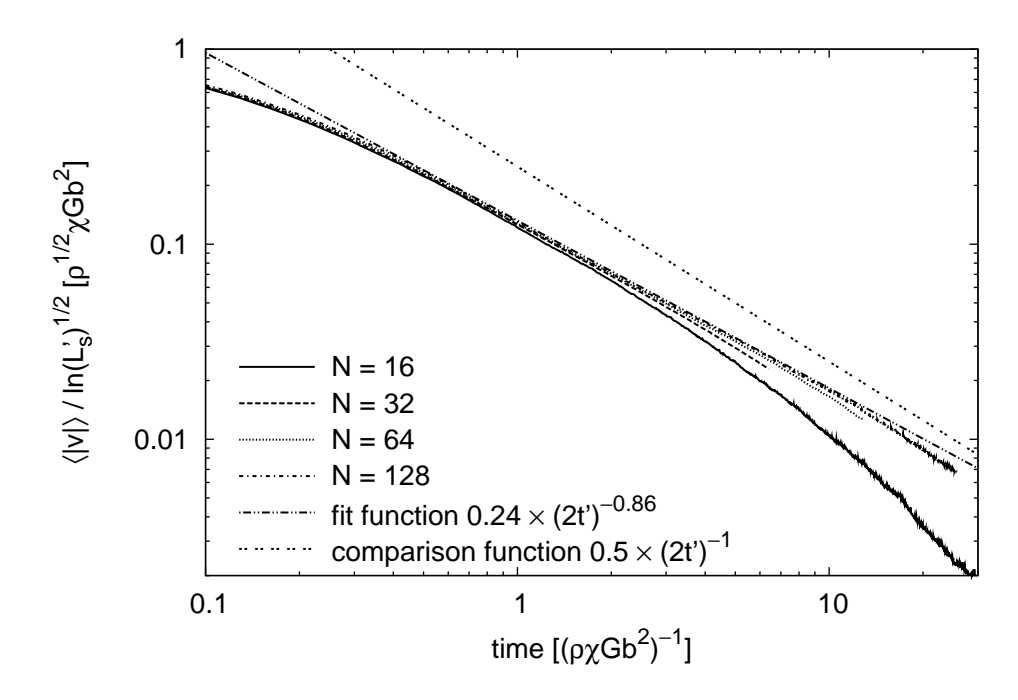


Figure 4. Evolution of the mean absolute velocity $\langle |v'| \rangle$ for different system sizes N at zero external stress.

Miguel and co-workers [4, 6], this is estimated to be ~ 0.1 in natural units. As it was demonstrated in figure 2, external stresses in this range do not appreciably change the evolution of the elastic energy. We study the relaxation of the strain rate mainly in order to assess, by comparing with the work of Miguel et al., the relevance of different initial conditions on the creep behaviour of dislocation systems.

Figure 5 shows the numerically determined evolution of the plastic strain rate $\dot{\gamma}'$ for different system sizes and external stress values. As can be seen, the plastic strain rate scales roughly in proportion with the external stress. The relaxation does not follow any discernible power law but is roughly exponential. This is in marked contrast with the findings of Miguel et al. [4, 6] who for well relaxed initial configurations demonstrate an Andrade-type power-law decay, $\dot{\gamma} \propto t^{-2/3}$. The discrepancy points to the crucial importance of initial conditions for relaxation processes in dislocation systems – a factor which is also borne out by the history dependence of creep relaxation processes that was demonstrated by Miguel et al. [6].

4.1.5. Role of boundary conditions (simulation box orientation). In this section we investigate the influence of different ways of implementing the periodic boundary conditions by tilting the angle between the edges of the simulation box and the trace of the slip planes. Simulations with different tilt angles φ are physically equivalent except for the spatial arrangement of the periodic images of each dislocation (see figure 6). This arrangement affects the dislocation–dislocation interactions on scales comparable to the simulation box size. Also, the interaction energy of each dislocation with its periodic

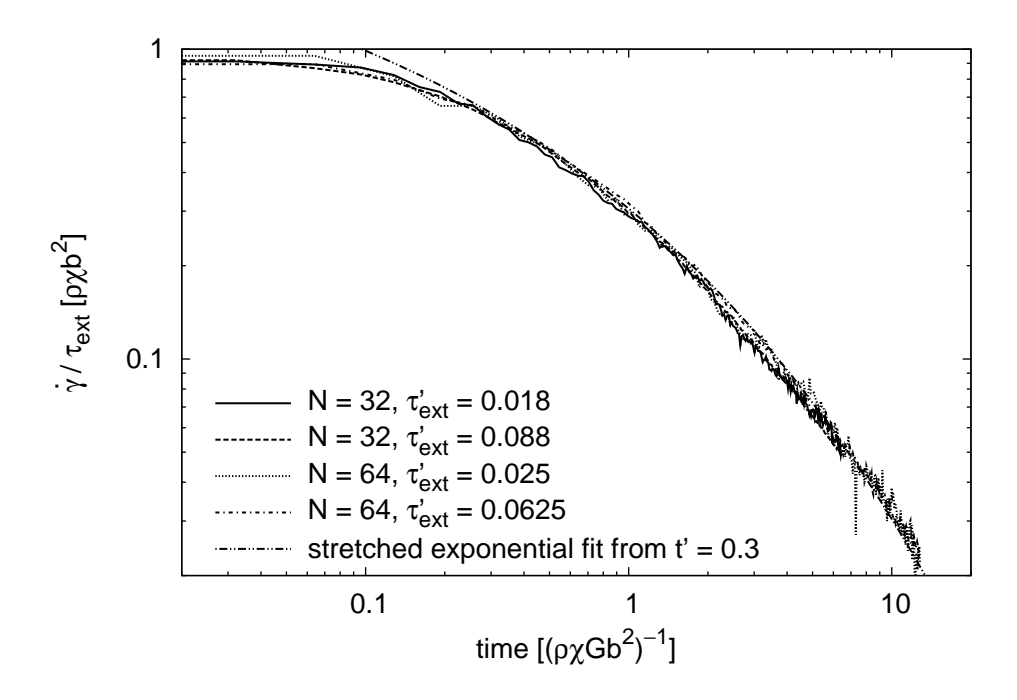


Figure 5. Evolution of the plastic strain rate $\dot{\gamma}'$ normalised with the external stress τ'_{ext} for different system sizes N and external stress values τ'_{ext} .

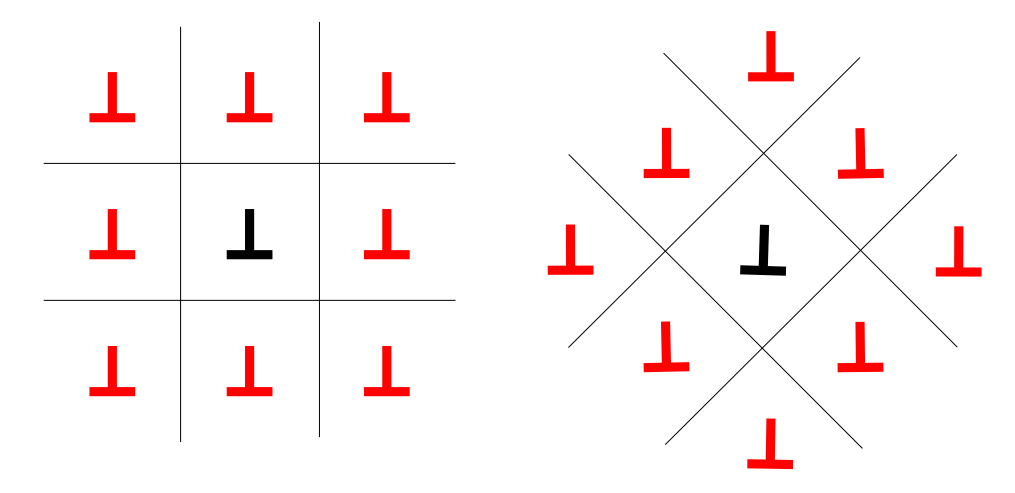


Figure 6. Arrangement of the first 8 periodic images of a given dislocation for $\varphi = 0^{\circ}$ (left) and $\varphi = 45^{\circ}$ (right). The latter configuration has a higher elastic energy as the nearest neighbours of each dislocation are in an energetically unfavourable configuration.

images affects the initial elastic energy of the system, which is smallest for $\varphi = 0$ and has a maximum for $\varphi = 45^{\circ}$.

The influence of simulation box orientation on the relaxation process is illustrated in figure 7. The absolute values of the squared velocity (or equivalently the energy dissipation rate) are higher for $\varphi = 45^{\circ}$ than for $\varphi = 0$. However, both curves differ only by a constant factor (the ratio of the initial excess energies), while the dynamics

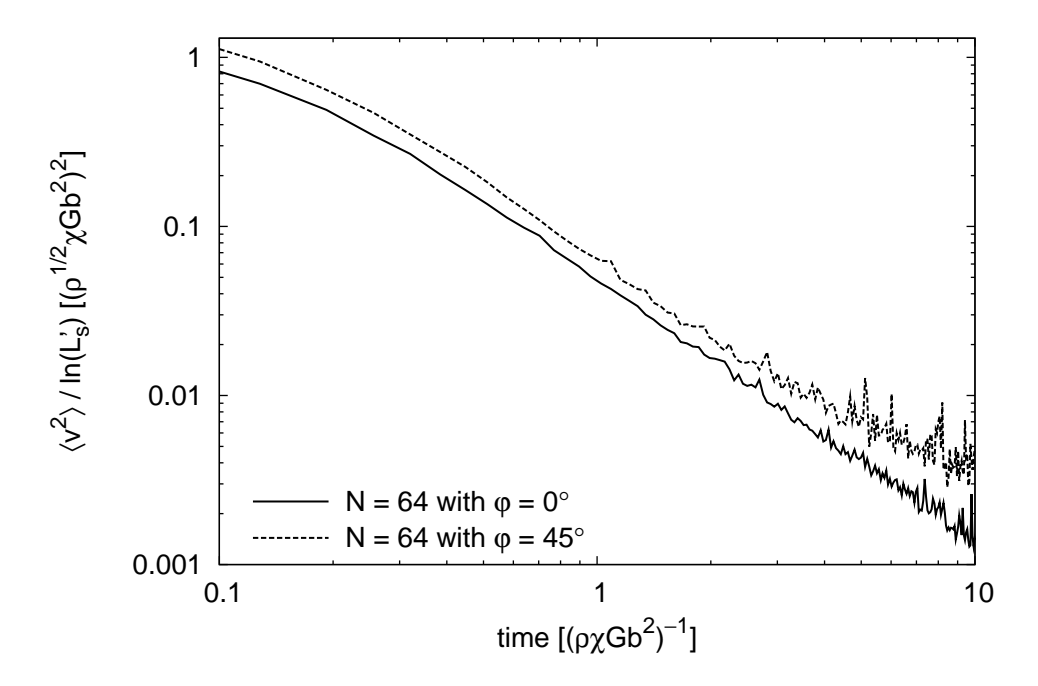


Figure 7. Evolution of the mean square velocity $\langle v'^2 \rangle$ in systems with a single slip geometry with the simulation box oriented at different angles φ to the slip planes.

of the relaxation processes is otherwise identical.

4.2. Relaxation of arrangements of dislocations of the same sign

For systems of dislocations of the same sign we have numerically evaluated the evolution of the mean square velocity $\langle v'^2 \rangle$ (or, equivalently, of the energy dissipation rate) and of the mean absolute velocity $\langle |v'| \rangle$. All calculations were performed at zero external stress since any applied stress would induce a sustained drift motion of the dislocation arrangement.

Results are shown in figure 8 and figure 9 together with the fit functions obtained for neutral dislocation arrangements (see figure 3 and figure 4). It is evident that the relaxation of same-sign dislocation systems follows the same scaling laws that have been observed for systems containing equal numbers of dislocations of both signs. This provides strong support for our basic conjecture that relaxation is governed by the stress-driven elimination of excess dislocations in a process that progresses from small to large scales. The processes occurring on short scales, on the other hand, are evidently different for the two systems (dipole formation vs. formation of walls). This is reflected by the fact that the relaxation process in the single-sign dislocation systems shows an initial size dependence which is not present in neutral dislocation systems (see figure 3 and figure 4 for comparison).

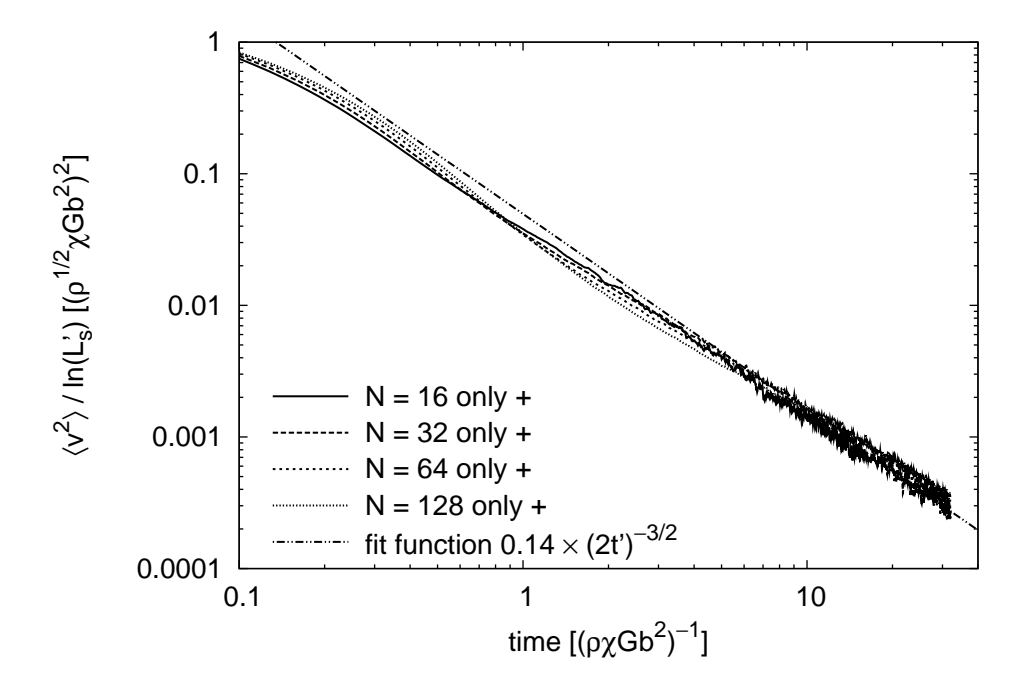


Figure 8. Evolution of the mean square velocity $\langle v'^2 \rangle$ for different system sizes N for dislocations of the same sign.

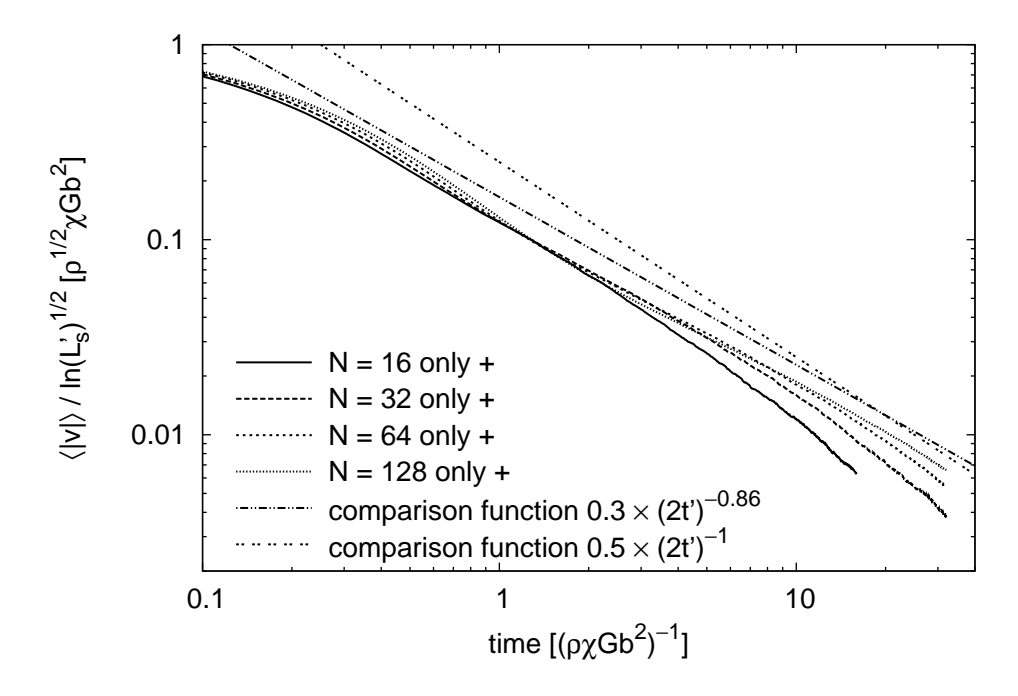


Figure 9. Evolution of the mean absolute velocity $\langle |v'| \rangle$ for different system sizes N for dislocations of the same sign.

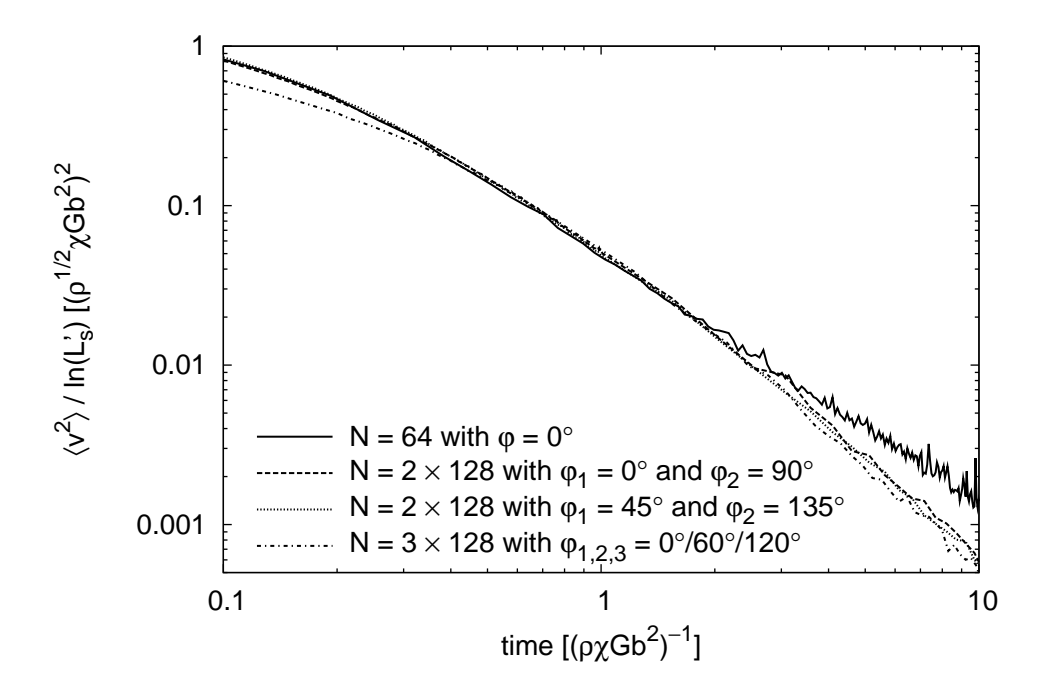


Figure 10. Comparison of the evolution of the mean square velocity $\langle v'^2 \rangle$ in dislocation systems with single and multiple slip geometries. In the figure, ρ means the total density of dislocations on all slip systems. The last two curves were shifted downwards to help comparison.

4.3. Dislocation relaxation on multiple slip systems

Figure 10 compares the relaxation of dislocation systems in single, double and triple slip. As seen in the figure, at long times the relaxation in multiple slip geometries accelerates in comparison with the relaxation in single slip. This is consistent with the idea that in multiple slip geometries relaxation processes proceed through the formation of dislocation locks and the annihilation of mobile dislocations at these locks. The long range stress fields associated with dislocation locks and the removal of dislocations accelerate the relaxation as seen in the figure. One of the main assumptions behind our scaling model, namely that the motion of mobile dislocations is governed mainly by their mutual interaction, no longer holds in multiple slip geometries. Therefore, the scaling model can not be applied to these situations. Indeed, as seen in figure 10, no power law relaxation regime can be detected in the multiple slip simulations.

5. Discussion and conclusions

The present paper discusses the relaxation of initially random arrangements of straight, parallel edge dislocations. Following a phenomenological analogy with the kinetics of bimolecular reactions [17] the relaxation process can be divided into three consecutive stages. Stage 1 is characterised by rapid rearrangements of neighbouring dislocations, leading to the formation of dipoles, multipoles, and/or short wall segments. Stage 2

hosts the gradual extinction of initial fluctuations in the Burgers vector density on ever increasing length scales through the long range transport of excess dislocations. This stage gives rise to characteristic power-law relaxation dynamics. The relaxation process terminates in stage 3 when the characteristic fluctuation length reaches the system size.

Our considerations focus on the power-law relaxation dynamics in stage 2. In section 3, we formulated a scaling theory for this process by making the analogy with a bimolecular reaction. To this end, we considered a highly simplified picture where pair interactions between positive and negative excess dislocations lead to long-range dislocation transport resulting in the formation of dislocation dipoles. This led to predictions for the evolution of the elastic energy and the first two moments of the dislocation velocity. These predictions were then compared to ensemble averages of discrete dislocation dynamics simulations, and convincing agreement was found for single slip geometries. For multiple slip geometries, however, the persistent long range stress fields of dislocation locks accelerate the relaxation process, to which the scaling model can no longer be applied.

The actual dislocation processes in many-dislocation systems are much more complex than the simplified picture underlying our scaling arguments. Instead of long-range transport of excess dislocations and dipole formation, we see complex rearrangements resulting in dislocation dipoles, multipoles, and walls. In addition, it is well known that dislocations have a propensity to form large-scale heterogeneous patterns consisting of dislocation-rich and dislocation depleted regions. In the following we briefly discuss how these complex static and dynamic features fit into the idealised picture we used in the previous sections.

5.1. Dipoles, multipoles and walls

We have developed our scaling argument for dipole formation which can be considered a bimolecular reaction between positive and negative dislocations. However, actual dislocation arrangements are much more complex. It is therefore important to emphasise that the core of the argument is the elimination of large-scale fluctuations in the excess Burgers vector density, and *not* the resulting arrangement of nearby dislocations. For the long-time asymptotics of the relaxation process, which is governed by the elimination of fluctuations on larger and larger scales, the small-scale arrangement of dislocations is virtually irrelevant – at least as long as the local features (dipoles, multipoles, short walls and combinations of all these) do not give rise to long-range stresses. According to the present argument, a well-screened dislocation arrangement is one in which Burgers vector fluctuations have been eliminated on all scales. If we are dealing with a neutral dislocation system (equal numbers of positive and negative dislocations) this means that the net Burgers vector is zero in each small volume, i.e., for each dislocation we can find exactly one partner of opposite sign nearby. This motivates the dipolar picture even if the actual dislocation arrangements may be more complex.

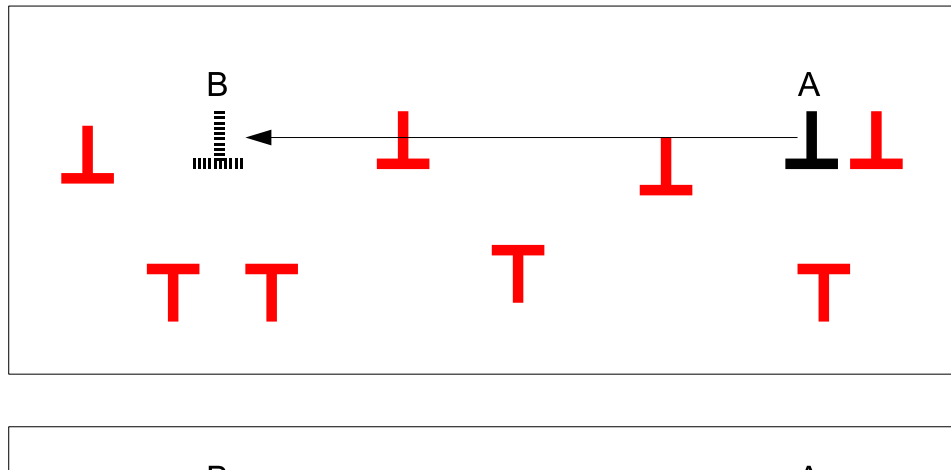
An alternative mechanism for creating well-screened dislocation arrangements is

the formation of system-spanning walls of dislocations of the same sign. arrangement of edge dislocations of one sign into a wall perpendicular to the glide plane removes the logarithmic divergence of the dislocation energy and introduces a screening length that is proportional to the dislocation spacing along the wall [15]. Walls are conspicuous both in simulations and in many experimentally observed dislocation microstructures. At first glance, wall formation mechanism seems to be completely at odds with the mechanism discussed in the present paper: Formation of walls of samesign dislocations increases, rather than reduces, the Burgers vector density fluctuations. However, a closer investigation reveals that wall formation by itself is not a screening mechanism at all. Forming a wall of randomly spaced dislocations does not reduce the energy in comparison with a random 2D dislocation arrangement (see Appendix). Instead, the screening effect is contingent on the equal spacing of dislocations, i.e. on suppressing fluctuations of the Burgers vector density along the wall direction. If we start from a random dislocation arrangement this is not easy to obtain: Either the dislocations must have climb degrees of freedom (which we do not consider in the present study), or dislocation motions that lead to the formation of multiple walls must be correlated over large distances such as to ensure that each wall collects only those dislocations that fit into an evenly spaced pattern. In the latter case, we are again dealing with the suppression of Burgers vector density fluctuations on all scales above the wall spacing, and the long time asymptotics of this process is expected to obey our scaling theory. This is confirmed by the simulations, which however also demonstrate that the short-time behaviour is different for neutral dislocation systems where the local arrangement of dislocations is characterised by dipolar and multipolar patterns, and for single-sign dislocation systems where the local arrangement of dislocations is characterised by walls (compare figure 3 and figure 8).

5.2. Long-range transport of excess dislocations

Our scaling argument considers the stress-driven long-range transport of excess dislocations. The picture underlying the argument is schematically shown in figure 11 (top): A positive excess dislocation at A is attracted by a negative excess dislocation at B and the two recombine by long-range motion which is not affected by the stress field of the dislocations in between A and B. The figure also indicates that this idealisation may not be feasible when we are dealing with multipolar arrangements rather than isolated narrow dipoles: In that case the mutual interaction of the excess dislocation may be much weaker than their interaction with other dislocations 'on the way'. As a consequence, recombination is much more likely to occur by a collective rearrangement as shown in figure 11 (bottom).

How does this affect our scaling argument? The total driving force for the process is the same in both cases. However, a collective rearrangement on scale L is likely to involve $N = L\sqrt{\rho}$ dislocations [N=3] in figure 11 (bottom)]. Hence the driving force per dislocation is reduced by a factor of the order of N. However, the same is true for



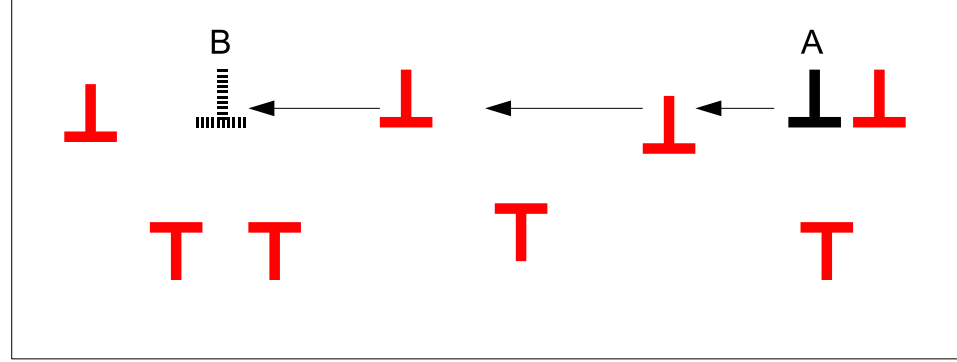


Figure 11. Schematic illustration of excess dislocation transport in a multipolar dislocation arrangement: a positive excess dislocation at A 'recombines' with a negative excess dislocation at B (top) by direct motion from A to B or (bottom) by collective rearrangement involving multiple dislocations.

the characteristic distance that has to be covered by each dislocation (L in the case of direct transport, $1/\sqrt{\rho}$ in the case of collective rearrangement). As we assume that the dislocation velocity is proportional to the driving force, it follows that the characteristic time scale for eliminating the excess dislocation is the same in both cases, and our scaling argument remains valid.

5.3. Large-scale dislocation patterning

It is a well known phenomenon that dislocation microstructures forming during plastic deformation form heterogeneous patterns consisting of regions of high and low dislocation density, with characteristic lengths that are large in comparison with the dislocation spacing. On a conceptual level, possible mechanisms underlying this patterning were discussed by Nabarro [20] who pointed out that it may be energetically favourable to 'segregate' the dislocation microstructure into areas of high and low density: If we are dealing with a well-screened dislocation arrangement, the energy density scales like $\mathcal{E} \propto \rho \ln(1/(b\sqrt{\rho}))$. In this case it can be easily shown that it is energetically favourable to increase ρ in some regions and decrease it proportionally in others. Such 'energetically driven' dislocation patterning could be a reason for the

formation of dislocation-dense and dislocation-depleted regions that is observed in many experiments. While this mechanism is not covered by the present model, it is not at variance with our considerations: In a neutral dislocation arrangement, the formation of dislocation-dense and dislocation-depleted regions might occur without disturbing the Burgers vector balance. We note, however, that in our simulations large-scale dislocation patterning is not observed – either because it does indeed not occur in single slip, or because the dislocation numbers in our simulations might be too small.

5.4. Conclusion

In conclusion we discuss the relevance of the processes discussed in the present paper for real-world systems. The relaxation of a random dislocation system has no direct counterpart in real deformation experiments, since it is impossible to 'prepare' such a random system in the first place. Our analysis of the screening of same-sign dislocation systems is, however, of general importance for understanding real dislocation patterns since it demonstrates that wall formation, though a conspicuous feature, can by itself not account for screening. This observation points to the importance of investigating long-range correlations between dislocation positions both within the walls and across different walls, and offers ample scope for future investigations.

The investigated processes are of significant importance for discrete dislocation dynamics simulations of plasticity as the slow nature of the relaxation makes it difficult to obtain well-defined and energetically stable initial configurations. Our comparison of strain-rate relaxation experiments with the results of Miguel et al. demonstrates that the collective behaviour of dislocation systems may depend significantly on initial conditions. The analysis of this dependence is still in its infancy, yet understanding it is indispensable for carrying out dislocation plasticity simulations in a controlled and well-defined manner.

Acknowledgments

Financial support of the Hungarian Scientific Research Fund (OTKA) under Contract No. K 67778, of the European Community's Human Potential Programme under Contract Nos. MRTN-CT-2003-504634 [SizeDepEn] and NMP3-CT-2006-017105 [DIGIMAT] and of NEST Pathfinder programme TRIGS under contract NEST-2005-PATH-COM-043386 are gratefully acknowledged.

Appendix: Calculation of the elastic energy of a random dislocation wall

We consider a wall of infinite height running along the plane x = 0 in an isotropic material. Edge dislocations of Burgers vector $\mathbf{b} = b\mathbf{e}_{\mathbf{x}}$ are distributed randomly along the wall with average linear density 1/h. The geometry corresponds to a plane-strain

situation, hence the elastic energy density can be written as

$$\mathcal{E} = \frac{1}{4\mu} \left[(\sigma_{xx} + \sigma_{yy})^2 (1 - \nu) + 2(\sigma_{xy}^2 - \sigma_{xx}\sigma_{yy}) \right]. \tag{A.1}$$

The total energy of the system is obtained by integrating (A.1) over the system volume,

$$E = \int_{V} \mathcal{E} d^{2}r = \frac{1 - \nu}{4\mu} \int_{V} (\sigma_{xx} + \sigma_{yy})^{2} d^{2}r, \tag{A.2}$$

where we have used that, for an infinite system, the second and third terms on the right-hand side do not contribute to the total energy. This can be shown as follows: For plane-strain deformation, the stresses can be written as derivatives of the Airy stress function χ , $\sigma_{xx} = \partial_y^2 \chi$, $\sigma_{yy} = \partial_x^2 \chi$ and $\sigma_{xy} = -\partial_x \partial_y \chi$. Hence,

$$\int_{V} [\sigma_{xy}^{2} - \sigma_{xx}\sigma_{yy}] d^{2}r = \int_{V} [\partial_{x}\partial_{y}\chi\partial_{x}\partial_{y}\chi - \partial_{x}^{2}\chi\partial_{y}^{2}\chi] d^{2}r.$$
(A.3)

Partially integrating the second term in the integral on the right-hand side with respect to x and y shows that this integral contributes only surface terms to the total energy. These terms are negligible in the infinite-system limit.

The ensemble-averaged stress at any point is given by summing over the stress fields of the individual dislocations in the wall and averaging over the different realizations of the random dislocation positions:

$$\langle \sigma_{ij}(\boldsymbol{r}) \rangle = \sum_{n} \langle \sigma_{ij}^{(n)}(\boldsymbol{r}) \rangle,$$
 (A.4)

where $\sigma_{ij}^{(n)}$ is the ij component of the stress created at \mathbf{r} by the nth dislocation. The elastic energy of the system depends on the averages of products $\langle \sigma_{ij}(\mathbf{r})\sigma_{kl}(\mathbf{r})\rangle$ where $(ij,kl) \in [(xx,xx);(xx,yy);(yy,yy)]$. In evaluating these averages we use that the y coordinates of the individual dislocations are independent random variables:

$$\langle \sigma_{ij}(\boldsymbol{r})\sigma_{kl}(\boldsymbol{r})\rangle = \langle \sigma_{ij}(\boldsymbol{r})\rangle\langle \sigma_{kl}(\boldsymbol{r})\rangle + \sum_{\boldsymbol{r}} \left[\langle \sigma_{ij}^{(n)}(\boldsymbol{r})\sigma_{kl}^{(n)}(\boldsymbol{r})\rangle - \langle \sigma_{ij}^{(n)}(\boldsymbol{r})\rangle\langle \sigma_{kl}^{(n)}(\boldsymbol{r})\rangle\right].$$
(A.5)

We now make the following observations:

- The average stresses $\langle \sigma_{ij}(\mathbf{r}) \rangle$ and their products $\langle \sigma_{ij}(\mathbf{r}) \sigma_{kl}(\mathbf{r}) \rangle$ depend on the x coordinate only.
- The average single-dislocation stresses $\langle \sigma_{xx}^{(n)} \rangle$ and $\langle \sigma_{yy}^{(n)} \rangle$ become zero in the limit $a \to \infty$, since these stresses are antisymmetric functions of the y coordinate. The same is true for the average total stresses $\langle \sigma_{xx} \rangle$ and $\langle \sigma_{yy} \rangle$.

With these observations and using (A.5) we can write the system energy as

$$E = \int_{V} \mathcal{E} d^{2}r = \sum_{n} \frac{1 - \nu}{4\mu} \int_{V} \langle (\sigma_{xx}^{(n)} + \sigma_{yy}^{(n)})^{2} \rangle d^{2}r$$
$$= NGb^{2}\pi (1 - \nu) \ln \left[\frac{L}{2b} \right], \tag{A.6}$$

where the second step follows by interchanging the averaging and the integration. L is the system size and N = L/h is the total number of dislocations in the system. It follows

from (A.6) that the energy per dislocation is equal to the energy of a single unscreened dislocation and, hence, equals the energy in a completely random 2D arrangement. In other words, the arrangement of dislocations of the same sign in a random wall does (with the possible exception of surface terms that are negligible in the infinite system limit) not produce any reduction of the total energy. Accordingly, the thermodynamic driving force towards forming such a wall is zero.

References

- [1] Zaiser M, Statistical modelling of dislocation systems, 2001 Mat. Sci. Eng. A 309–310 304–15
- [2] Groma I, Csikor F F and Zaiser M, Spatial correlations and higher-order gradient terms in a continuum description of dislocation dynamics, 2003 Acta Mater. 51 1271–81
- [3] Zaiser M, Scale invariance in plastic flow of crystalline solids, 2006 Adv. Phys. 55 185–245
- [4] Miguel M C, Vespignani A, Zaiser M and Zapperi S, Dislocation jamming and Andrade creep, 2002 Phys. Rev. Lett. 89 165501
- [5] Miguel M C, Moretti P, Zaiser M and Zapperi S, Statistical dynamics of dislocations in simple models of plastic deformation: Phase transitions and related phenomena, 2005 Mat. Sci. Eng. A 400–401 191–8
- [6] Miguel M C, Laurson L and Alava M, Material yielding and irreversible deformation mediated by dislocation motion, 2008 Eur. Phys. J. B 64 443–50
- [7] Wilkens M, Das Spannungsfeld einer Anordnung von regellos verteilten Versetzungen, 1967 Acta Met. 15 1412-7
- [8] Wilkens M, Das mittlere Spannungsquadrat ⟨σ²⟩ begrenzt regellos verteilter Versetzungen in einem zylinderförmigen Körper, 1969 Acta Met. 17 1155–9
- [9] Zaiser M, Miguel M-C and Groma I, Statistical dynamics of dislocation systems: The influence of dislocation-dislocation correlations, 2001 Phys. Rev. B 64 224102
- [10] Zaiser M and Seeger A, Long-range internal stresses, dislocation patterning and work hardening in crystal plasticity, 2002, Dislocations in Solids Vol. 11, ed F R N Nabarro and M S Duesbery (Elsevier)
- [11] Csikor F F and Groma I, Probability distribution of internal stress in relaxed dislocation systems, 2004 Phys. Rev. B **70** 064106
- [12] Krivoglaz M A 1969 Theory of x-ray and thermal neutron scattering by real crystals (New York: Plenum)
- [13] Csikor F F, Kocsis B, Bakó B and Groma I, Numerical characterisation of the relaxation of dislocation systems, 2005 Mat. Sci. Eng. A 400-401 214-7
- [14] Csikor F F and Zaiser M, Scaling and glassy dynamics in the relaxation of dislocation systems, 2006 Proc. Int. Conf. on Statistical Mechanics of Plasticity and Related Instabilities (29 August– 2 September 2005 Bangalore) ed M Zaiser et al (Proceedings of Science) 058
- [15] Hirth J P and Lothe J 1982 Theory of Dislocations (New York: Wiley-Interscience)
- [16] Bakó B, Groma I, Györgyi G and Zimányi G, Dislocation patterning: The role of climb in mesoscale simulations, 2006 Comp. Mater. Sci. 38 22–8
- [17] Ovchinnikov A A and Zeldovich Ya B, Role of density fluctuations in bimolecular reaction kinetics, 1978 Chem. Phys. 28 215–8
- [18] Groma I, Györgyi G and Kocsis B, Debye screening of dislocations, 2006 Phys. Rev. Lett. 96 165503
- [19] Thomson R, Koslowski M and LeSar R, Energetics and noise in dislocation patterning, 2006 Phys. Rev. B 73 024104
- [20] Nabarro F R N, Complementary models of dislocation patterning, 2000 Phil. Mag. A 80 759–64